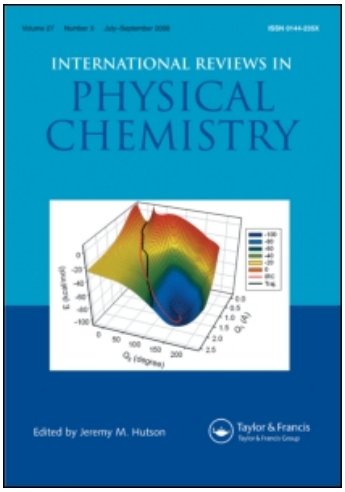

International Reviews in Physical Chemistry
Publication details, including instructions for authors and subscription information:
http://www.informaworld.com/smpp/title~content=t713724383

One-electron resonances in electron scattering from polyatomic molecules

Robert R. Lucchese[a]; F. A. Gianturco[b]
[a] Department of Chemistry, Texas A&M University, College Station, Texas, USA [b] Department of Chemistry, The University of Rome, Citta Universitaria, Italy

To cite this Article Lucchese, Robert R. and Gianturco, F. A.(1996) 'One-electron resonances in electron scattering from polyatomic molecules', International Reviews in Physical Chemistry, 15: 2, 429 — 466
To link to this Article: DOI: 10.1080/01442359609353190
URL: http://dx.doi.org/10.1080/01442359609353190

INTERNATIONAL REVIEWS IN PHYSICAL CHEMISTRY, 1996, VOL. 15, NO. 2, 429–466

One-electron resonances in electron scattering from polyatomic molecules

by ROBERT R. LUCCHESE† and F. A. GIANTURCO‡

† Department of Chemistry, Texas A&M University, College Station, Texas 77843-3255 USA

‡ Department of Chemistry, The University of Rome, Città Universitaria, 00185, Italy

One-electron resonances in electron scattering from polyatomic molecules were examined using set of interconnected models. We compared resonant states predicted from the virtual orbitals of a minimum-basis-set self-consistent-field (MBS-SCF) calculation with scattering resonances found using both a purely local model potential for the electron–molecule interaction based on an adiabatic separation of the angular and radial motion and a more accurate exact-static-exchange-plus-model-correlation–polarization interaction potential. Considering electron scattering from N_2, SF_6, and C_6H_6, we found that the MBS-SCF virtual orbitals were an excellent predictor of the symmetry and approximate location of one-electron resonances. The adiabatic radical potentials were very useful in understanding the mechanism for resonant trapping, although strong non-adiabatic coupling sometimes required more than one adiabatic potential to be considered to accurately represent the resonant dynamics. The essential feature of the trapping mechanism for each of these systems was an angular momentum barrier found in one of its adiabatic potentials.

1. Introduction

Electron–molecule scattering is an elementary step in a wide variety of important processes and systems. These include processes in areas such as astrophysics, planetary atmospheres, lasers, and radiation physics. An example of an area of intense current interest is given by electron–molecule scattering processes which occur in cold plasmas used for a wide variety of materials processing, including semiconductor device fabrication (Grill 1994). Thus there is a continuing effort to develop the necessary experimental and theoretical tool for studying these processes (Shimamura and Takayanagi 1984).

Electrons scattering from molecules can be subject to a number of resonant processes. Within the Born–Oppenheimer approximation, electronic motion is often assumed to occur on a time-scale which is short compared to molecular vibrations. However, there are a number of instances where this assumption breaks down. For example, as a scattering electron leaves the vicinity of the target molecule, if the electron is moving slowly enough, the time-scale for electronic and nuclear motion can be comparable. A particularly dramatic example of the breakdown of the Born–Oppenheimer approximation is the case of scattering from a molecule with a dipole moment. In the fixed nuclei (FN) approximation, the total cross-section diverges due to the long range of the electron–dipole interaction. However, when the rotational motion of the molecule is included in the scattering problem, the averaging of the interaction potential over the rotation of the molecule removes the divergence in the total cross section (Garret 1972).

0144–235X/96 $12·00

Within the FN approximation one can use the Hartree–Fock (HF) approximation to qualitatively describe electron-scattering resonances. The positive-energy canonical HF orbitals are exactly the one-electron wavefunctions for scattering from an N electron closed shell target within the static-exchange approximation (Lane 1980). In general the canonical HF orbitals provide a good one-electron basis set for expanding the full $N+1$ electron scattering state. The unoccupied HF orbitals are usually referred to as virtual orbitals.

In electron–molecule scattering, if the target state can be accurately represented by the HF wavefunction, the asymptotic scattering state can be described by a single Slater determinant formed from the antisymmetrized product of the occupied HF orbitals and one additional positive energy scattering orbital. The resonant processes can then be characterized by the number of electron excitations and de-excitations needed to obtain the resonant state from the single determinant asymptotic scattering state. Most resonances involve only one or two-electron excitations or de-excitations (Burke 1968, Hall and Read 1984, McDaniel 1989). A typical two-electron resonance is characterized by a quasi-bound electronic state which decays into the scattering continuum by two electrons changing orbitals, e.g. with two electrons initially in excited bound orbitals, one electron drops to a lower bound orbital and the other electron is excited into the continuum. A one-electron resonance is characterized by an $N+1$ electron state where a single electron is in a one-electron state above the energy required to leave the system but is temporarily trapped either by a dynamic or static barrier.

Experimentally, a resonance causes a modulation in the scattering cross-section as a function of the scattering energy. If there is little background scattering, the resonance will yield an isolated peak in the cross-section (Taylor 1972). In addition to causing a peak in the elastic cross-section, one-electron resonances also are an important mechanism for vibrational excitation of molecules (Herzenberg 1984). The resonant vibrational excitation process can be illustrated by assuming that a molecule is initially in its ground state. Then when the electron becomes temporarily trapped in the resonant state, the nuclei of the molecule begin to move on the Born–Oppenheimer potential energy surface which is characteristic of the negative ion. Usually the ground state and negative ion state potentials are displaced with respect to one another, thus on the potential of the negative ion in the nuclei find themselves in a vibrationally excited state. Depending on the lifetime of the resonance this can lead to a vibrational excitation of the molecule when the electronic state decays back to the ground state through ejection of the trapped electron.

Theoretically, a resonance is characterized by the asymptotic phase shift of the scattered wave rising rapidly through π as a function of the scattering energy (Taylor 1972). This rapid rise in the eigenphase sum can be shown to be characteristic of a time delay in the scattering process, i.e. the scattered electron is temporarily trapped in the vicinity of the molecule. The scattering process can also be characterized by the energy dependence of the **S** scattering matrix. By analytically continuing this matrix to complex energies, one can show that the rapidly rising phase shift at real energies is due to a pole of the **S** matrix near the real energy axis in the lower half of the complex energy plane at an energy E given by

$$E = R_R - i\frac{\Gamma}{2}, \tag{1}$$

where E_R is the energy and Γ is the width of the resonance.

This paper is concerned with low energy one-electron resonances in electron–

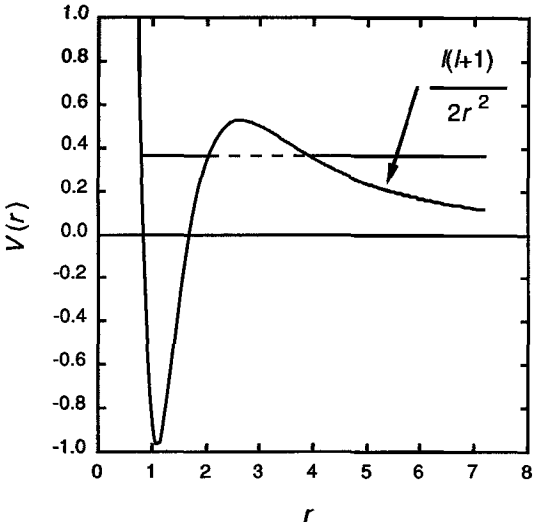

Figure 1. Schematic illustration of an angular momentum barrier resonance. The energy of the resonant state is indicated by the horizontal line.

molecule scattering. We will examine when they typically occur in electron–molecule scattering and what the mechanism is for the trapping of the electron. In atomic systems and in small molecule systems where there is spherical (or near spherical) symmetry the one-electron scattering problem is decoupled into states which are eigenfunctions of the angular momentum. For a given value of the angular momentum the differential equation for the radial wave function then contains an effective radial potential of the form (in atomic units)

$$V_l^{\text{eff}}(r) = V(r) + \frac{l(l+1)}{2r^2}. \tag{2}$$

If the spherically symmetric potential $V(r)$ is attractive, then for some values of $l > 0$ it is possible that the potential has an inner well with a barrier through which an electron can escape to large r, as schematically illustrated in figure 1. For such a potential, it is then possible to have a pseudo-bound state of the potential at positive energies which can slowly decay as the electron escapes through the potential barrier by tunnelling. Due to the relationship between the shape of the potential and the resonant state such one-electron resonances are referred to as 'shape resonances' (McDaniel 1989).

In molecular systems in the FN approximation, the interaction potential between the scattered electron and the target is not spherically symmetric. Although it is sometimes useful to think qualitatively of the interaction potential as being spherically symmetric, the non-spherical part of the potential couples states of different angular momenta, generally shortening the lifetime of any resonant state.

One mechanism for trapping resonant states in molecular systems which has been proposed (Dehmer 1972, Swanson *et al.* 1981) for systems with electronegative atoms is trapping by a potential barrier due to a repulsive interaction with the electron-rich electronegative atoms. This repulsive interaction would be purely electrostatic in nature and thus not dependent on high angular momentum for the trapping. However, as has been pointed out previously (Natoli 1983), for a system such as SF_6 a calculation of the interaction potential reveals that the potential is purely attractive so that electrostatic

interactions cannot provide the required barrier for trapping the electron. Note that for systems of lower symmetry than that possessed by SF_6 there will be some directions of electron motion in which there is an electrostatic barrier. However, there is not a definitive example where electrostatic barriers have been shown to be the source of the trapping of a resonant state.

A refinement of the radial angular momentum barrier model for molecular shape resonances is the adiabatic potential model (Le Dourneuf *et al.* 1982, Lan *et al.* 1983, Battaglia and Gianturco 1989, Gianturco 1992). In this approach an effective radial potential is obtained by making an adiabatic separation of the angular and radial modes. Thus, within a single-centre expansion, at each r an angular Schrödinger equation is solved. The eigenvalues of the angular motion at that r are then the values of the adiabatic radial potential at that r. Excluding the case of the dipole scattering problem, the adiabatic potentials coincide with the usual single-centre-expanded effective radial potentials at large and small values of r since in those limits the angular momentum term dominates the angular Hamiltonian. In the simplest approximation, the non-adiabatic radial coupling is ignored and the resonance is just obtained as a pseudo-bound state on a single adiabatic potential trapped behind an angular momentum barrier. This approach can explain the trapping mechanism of many molecular shape resonances, however as we will illustrate below for e–N_2 and e–SF_6 scattering, the non-adiabatic couplings can be crucial elements in the mechanism for trapping the resonant electron. An additional limitation of this approach is that it can be most simply implemented and interpreted for purely local potentials, while it is well known that an accurate representation of the exchange interaction necessarily requires the inclusion of non-local potentials (Morrison and Collins 1981). Here we will give some illustrative examples where we used an appropriate model potential to understand the molecular shape resonance on a semi-quantitative level, although such an approach could not in general reproduce all quantitative details of the scattering with the full non-local potential.

Another approach which has been suggested for understanding the appearance of shape resonances in electron–molecule scattering is to examine the virtual HF orbitals which are obtained by performing the HF calculation in a one-electron basis set limited to a single atomic centred basis function for each core and valence atomic orbital of the constituent atoms of the molecule (Gianturco *et al.* 1972, Langhoff 1984). We will refer to this calculation as a minimum basis set self-consistent field (MBS-SCF) calculation. With the additional proviso that for second row atoms (Na–Ar) and below in the periodic table, the set of orbitals found in this fashion seem to include states which strongly resemble the shape resonant states. Langhoff and coworkers (Sheehy *et al.* 1989) have given examples where the MSB-SCF virtual orbitals provide a good representation of the resonant state within the Feshbach–Fano formalism. The concept of partitioning the scattering wavefunction into a resonant part and a non-resonant part, which is the basis of their approach, can provide a framework for computing resonant lifetimes and cross-sections, however, it does not provide any insight into the mechanism of trapping in the one-electron scattering resonances in electron–molecule scattering.

In this paper we report the results of studies of the occurrence of negative-ion shape resonances in a few representative systems (N_2, SF_6, C_6H_6). We used an accurate numerical scattering method to establish the existence and width of the resonances. We then examined in detail the relationship between these resonances and the resonances found on a local model potential. The resonances on the local model potential were

located using the analytic properties of the S matrix and previously developed pole finding methods (Stratmann and Lucchese 1992). The resonant state at the complex energy was then compared to the MBS-SCF virtual orbitals. Finally, a detailed analysis of the solution of the adiabatic radial potential model, with non-adiabatic couplings, revealed the combination of static and dynamic features which were important in trapping the resonant state.

2. Methodology

The nature of electron–molecule shape resonances was studied using a static-exchange-correlation-polarization (SECP) FN scattering calculation as our most accurate calculation. The resulting scattering equations were solved using a single-centre-expansion method which has been described in detail elsewhere (Gianturco and Jain 1986, Gianturco *et al.* 1994). In the present paper we will only outline the procedure used. Although this level of calculation reproduced the main features of the scattering process at low energy, it was difficult to analyse the qualitative aspects of the scattering process due to the complexity of the numerical model. In order to obtain a clear picture of the resonant process we also performed somewhat simplified model calculation.

2.1. *Fixed-nuclei scattering equations*

The electron–molecule scattering problem is significantly complicated by the need to couple the vibrational motion with the motion of the scattered electron. Although the Born–Oppenheimer approximation may be appropriate to describe the bound electrons in the system, at low energy the continuum electron can be strongly coupled to the nuclear kinetic energy. However, the essential nature of the shape resonance can still be examined using the FN approximation since the resonant state involves the scattered electron being temporarily trapped near the nucleus where the FN approximation is most valid for the scattered electron (Chang and Fano 1972). In the FN approximation the Schrödinger equation for the electronic motion is given by

$$H\Psi(r,X) = E\Psi(r,X), \tag{3}$$

where

$$H = \hat{T} + \hat{V} + \hat{H}_{\text{targ}}. \tag{4}$$

In equation (4) $\hat{T}$ is the kinetic energy operator of the incident electron and $\hat{V}$ is the interaction with the target given by

$$\hat{V} = \sum_{j=1}^{N} |r - x_i|^{-1} + \sum_{\gamma=1}^{M} Z_\gamma |r - R_\gamma|^{-1}, \tag{5}$$

H_{targ} is the electronic Hamiltonian for the target electrons, and r is the position of the continuum electron. The symbol X represents collectively the coordinates of the target electrons $x_i (i = 1, \ldots, N)$ while the positions of the nuclei with charge Z_γ are denoted by $R_\gamma (\gamma = 1, \ldots, M)$. The electronic Schrödinger equation is then reduced to a set of coupled one-particle equations by expanding the total electronic wavefunction Ψ in eigenstates of the target Hamiltonian as

$$\Psi(r,X) = \sum_{\alpha} \mathscr{A}\{\psi_\alpha(r)\phi_\alpha(X)\}, \tag{6}$$

such that

$$\hat{H}_{\text{targ}}\phi_\alpha(X) = \varepsilon_\alpha\phi_\alpha(X), \tag{7}$$

where $\mathscr{A}$ is the antisymmetrization operator and ε_α is the electronic eigenvalue for the α asymptotic target state. Inserting equation (6) into equation (3), multiplying on the left with the conjugate of one of the target eigenstates, and integrating over the target electron degrees of freedom leads to coupled partial integro–differential equations (IDEs) of the form

$$[\tfrac{1}{2}\nabla^2 + (E - \varepsilon_\alpha)]\psi_\alpha(r) = \sum_\beta \int V_{\alpha\beta}(r, r')\psi_\beta(r')\,\mathrm{d}^3r'. \tag{8}$$

The kernel of the integral operator for the potential, $V_{\alpha\beta}$, is in general a sum of diagonal (local potentials) and non-diagonal (non-local potentials) terms. The explicit expression for $V_{\alpha\beta}$ then depends on the form of the target states used in the expansion given in equation (6).

2.2. *Single-centre expansion*

There are a variety of ways for solving the scattering equations given in equation (8). Usually, the target states are computed using standard bound state methods where the one-electron functions are constructed from atomic centred basis functions (Hehre *et al.* 1986). This approach has been adapted to the scattering problem in several ways including the Schwinger-multichannel method (Takatsuka and McKoy 1981, Lucchese *et al.* 1986) and the complex-Kohn method (Schneider and Rescigno 1988).

Alternatively, there are a number of single-centre expansion methods which have been developed where all three-dimensional scattering functions are expanded in a set of symmetry adapted angular functions and where the corresponding radial functions are represented on a numerical grid (Gianturco and Jain 1986). In this approach an arbitrary three-dimensional function $F^{p\mu}(r, \theta, \phi)$ is expanded as

$$F^{p\mu}(r, \theta, \phi) = \sum_{lh} r^{-1} f^{p\mu}_{lh}(r) X^{p\mu}_{lh}(\theta, \phi), \tag{9}$$

where the function transforms as the μth element of the pth irreducible representation (IR) of the point group of the molecule. The functions $X^{p\mu}_{lh}$ are generalized harmonic functions which are eigenfunctions of L^2 given by symmetry-adapted linear combinations of the spherical harmonics $Y_{lm}(\theta, \phi)$ of the form

$$X^{p\mu}_{lh}(\theta, \phi) = \sum_m b^{p\mu}_{lhm} Y_{lm}(\theta, \phi). \tag{10}$$

Further details about the computation of the $b^{p\mu}_{lhm}$ have been given elsewhere (Gianturco *et al.* 1994).

Once all three-dimensional functions have been expanded using equation (9), the scattering equations given in equation (8) are reduced to a set of ordinary linear IDEs of the form

$$\left[\frac{1}{2}\frac{\mathrm{d}^2}{\mathrm{d}r^2} + (E - \varepsilon_\alpha)\right]\psi_{lh\alpha}(r) = \sum_{l'h'\beta} \int_0^\infty V_{lh\alpha, l'h'\beta}(r, r')\psi_{l'h'\beta}(r')\,\mathrm{d}r'. \tag{11}$$

2.3. *Static exchange potential*

One simple approximation for the target wavefunctions is to write $\phi_\alpha(X)$ as a single Slater determinant constructed from a product of one-electron molecular orbitals. Within that approximation one can apply the variation principle for the energy to obtain

the best one-electron functions. This procedure yields the HF wavefunction for the target state. If the one-electron functions are expanded in a finite one-electron basis set, the solution which produces the lowest variation energy is referred to as the self-consistent-field (SCF) solution (Schaefer 1972).

Using the HF or SCF solution for the target and truncating the expansion over target states in equation (6) to one state leads to the static-exchange (SE) approximation for the potential in equation (8) (Lane 1980). For a target which has a closed shell electronic structure with n_{occ} doubly occupied orbitals, ϕ_i, this potential can be written as

$$V_{\text{SE}} = \sum_{\gamma=1}^{M} Z_\gamma |r - R_\gamma|^{-1} + \sum_{i=1}^{n_{\text{occ}}} 2\hat{J}_i - \hat{K}_i, \tag{12}$$

where $\hat{J}_i$ is the usual local static potential defined by

$$\hat{J}_i(r_1) = \int \frac{\phi_i^*(r_2)\phi_i(r_2)}{r_{12}} \, \mathrm{d}^3 r_2, \tag{13}$$

and $\hat{K}_i$ is the non-local exchange potential operator defined by

$$(\hat{K}_i\psi)(r_1) = \phi_i(r_1) \int \frac{\phi_i^*(r_2)\psi(r_2)}{r_{12}} \, \mathrm{d}^3 r_2. \tag{14}$$

Electron–molecule scattering cross-sections computed using the Se potential are usually in fairly good agreement with experimental total scattering cross-sections. However, a major deficiency in the SE model for studying negative ion resonances is the lack of target response, i.e. electron correlation, in the scattering process. At higher energies, this is reflected in the fact that electronically inelastic processes are not obtained in the single-channel SE approximation. Such effects can be studied with the distorted-wave approximation using the SE wavefunctions as the distorted waves (Lee *et al.* 1982). Alternatively additional target states can be included in the expansion of the wavefunction. At low energies, the lack of target response leads to the neglect of important polarization effects. This can significantly alter the energy and width of resonances which occur below a scattering energy of $\sim 10\,\text{eV}$.

2.4. *Model correlation-polarization potential*

Target polarization can be included in a number of ways. The most straightforward approach is to include more states in the wavefunction expansion. These additional states can be either eigenstates of H_{targ} or they can be chosen to be pseudo-states whose inclusion accurately reproduce the static and low-frequency polarizability of the system (Burke and Mitchell 1974, Schneider 1977). A second approach is to include the appropriate optical potential. Such a potential can be computed by purely *ab initio* means (Klonover and Kaldor 1978). An alternative approach which we have used is to include the effects of correlation and polarization through the addition of a local, energy-independent model potential $V_{\text{CP}}(r)$ (Perdew and Zunger 1981, Padial and Norcross 1984, Gianturco *et al.* 1987). Briefly, this potential contains a short-range correlation potential smoothly connected to a long-range polarization potential. The short-range correlation potential V_{C} is obtained by defining an average correlation energy of a single particle, within the formalism of the Kohn and Sham variation theorem, and by obtaining the short-range correlation forces as an analytic function of the target electron density. The long-range polarization potential V_{P} is obtained by first constructing a model polarization potential which asymptotically agrees with the potential obtained from the static polarizability α of the molecule (Gianturco *et al.*

1994). This corresponds to including the first term in the second-order perturbation expansion of the polarization potential. This model potential can be either constructed assuming a single polarization centre, or by partitioning the static polarizability to different centres giving the form

$$V_P(r) = -\sum_{\gamma=1}^{M} \frac{\alpha_\gamma}{2|r - R_\gamma|^4}, \tag{15}$$

where the individual atomic polarizabilities are estimated using analogous molecules subject to the constraint that the total molecular polarizability is reproduced, i.e.

$$\alpha = \sum_{\gamma=1}^{M} \alpha_\gamma. \tag{16}$$

In general the long-range potential given in equation (15) does not exactly match the short-range potential V_C at any given value of r. To select an appropriate matching radius, r_{match}, to connect these two potentials, we first expand both V_P and V_C in a single-centre expansion. Then we find the radii where the two $l = 0$ radial potentials intersect. In all cases considered to date, these potentials cross at two values of r. Empirically we found that the best matching radius is the smaller of these two radii where the $l = 0$ potentials cross. Then the final definition for the model correlation-polarization potential is

$$V_{CP}(r) = \begin{cases} V_C(r), & r < r_{match}, \\ V_P(r) + \sum_{lm} \frac{c_{lm}}{r^{\lambda(l)}} Y_{lm}(\theta, \phi), & r \geqslant r_{match}, \end{cases} \tag{17}$$

where the values of c_{lm} have been determined so that potential is continuous at r_{match} and where $\lambda(l)$ is a function of l such that $\lambda = 6, 5, 6$ for $l = 0, 1, 2$ and $\lambda(l) = l + 2$ for $l \geqslant 3$. The function $\lambda(l)$ was chosen so that the term added to V_P has the same functional form as the first term neglected in the perturbation expansion of V_P. The static-exchange correlation-polarization (SECP) scattering potential we then used for the full scattering problem V_{SECP} was just the sum of the V_{SE} defined in equation (12) and V_{CP} defined in equation (17).

2.5. *Model exchange potential*

Although we solved the scattering problem using V_{SECP} we also utilized a purely local approximation to this potential where the non-local exchange potential was replaced by an approximate local model exchange (ME) potential denoted by V_{ME}. For this purpose we have used the Hara free-electron-gas-exchange (HFEGE) potential (Hara 1967, Salvini and Thompson 1981). In V_{ME}, the exchange interaction is approximated by an energy-dependent local function of the electron density of the target. We found that the energy dependence of the HFEGE potential was fairly weak so that scattering results over a given range of energies where the mean energy was used in the HFEGE potential were very similar to the results where the actual scattering energy was used to compute the HFEGE potential. As discussed below, we have used both of these forms of the HFEGE potential. The potential where the model exchange was used in place of the exact exchange will be referred to as the static-model-exchange-correlation-polarization (SMECP) potential V_{SMECP}. When a fixed energy is used in the model exchange potential we will indicate the energy in eV. For example the SMECP potential with a fixed energy of 15 eV used to compute the HFEGE potential will be

denoted $V_{SME(15)CP}$. The HFEGE potential is known to give fairly reliable results when compared to SE results, however the HFEGE tends to be somewhat less attractive than the true non-local exchange potential (Morrison and Collins 1981).

2.6. *Solution of the scattering equations*

The scattering cross-sections corresponding to a given solution of the scattering equations given in equations (11) can be obtained using a variety of approaches. When the scattering potential is purely a local potential, standard differential equation integrators can be used to obtain the wavefunction (Lesser 1968). The asymptotic form of the wavefunction is then analysed to obtain the appropriate scattering matrix from which total and differential cross-sections can be computed. When the potential given in equation (11) contains non-local terms an alternative approach must be used. We have developed a particularly powerful approach based on the Schwinger variational expression for the scattering matrix with Padé approximant corrections (Lucchese and McKoy 1983, Gianturco *et al.* 1994).

In the Schwinger–Padé approach, the total scattering potential V_T is written as the sum of an approximate local potential V_L and the difference between the local approximation and the full non-local potential which is denoted by V_D. Thus to obtain the cross-section with $V_T = V_{SECP}$ we used $V_L = V_{SMECP}$ so that the difference potential is $V_D = V_{SECP} - V_{SMECP}$. Equation (11) can then be transformed into an integral equation of the form

$$\psi_p = \phi_p + G_L V_D \psi_p, \tag{18}$$

where ϕ_p is a solution of the purely local potential problem

$$H_L \phi_p = E\phi_p. \tag{19}$$

The local Hamiltonian is given by $H_L = -\frac{1}{2}\nabla^2 + V_L$ and the Green function is defined by

$$(E - H_L)G_L = 1. \tag{20}$$

Using the **K** matrix to define the asymptotic form of the scattering solutions, we can then write the **K** matrix for the full potential as

$$K_{pq} = K_{pq}^{(L)} + K_{pq}^{(D)}, \tag{21}$$

where $\mathbf{K}^{(L)}$ is the **K** matrix due to scattering from V_L and $\mathbf{K}^{(D)}$ is the correction term which can be obtained from

$$K_{pq}^{(D)} = -2\langle \phi_p | V_D | \psi_q \rangle. \tag{22}$$

The expression for the correction to the **K** matrix given in equation (22) can be expanded using the Born series to give

$$K_{pq}^{(D)} = -2 \sum_{i=0}^{\infty} \langle \phi_p | V_D (G_L V_D)^i | \phi_q \rangle. \tag{23}$$

Using numerical techniques previously discussed (Gianturco *et al.* 1994), it is possible to compute the action of the G_L and V_D on any arbitrary function and thus to obtain all of the matrix elements given in equation (23). The convergence of this sum can be

greatly enhanced by using the [N/N] Padé approximant of the form

$$K_{pq}^{(D)}[N/N] = -2\sum_{i,j=0}^{N-1}\langle\phi_p|V_D(G_LV_D)^i|\phi_q\rangle D_{ij}^{-1}\langle\phi_p|V_D(G_LV_D)^j|\phi_q\rangle, \quad (24)$$

where D_{ij}^{-1} is the (i,j)th element of $\mathbf{D}^{-1}$ which is the inverse of the matrix $\mathbf{D}$ with elements

$$D_{ij} = \langle\phi_p|V_D(G_LV_D)^{i+j} - V_D(G_LV_D)^{i+j+1}|\phi_q\rangle. \quad (25)$$

The expression for the **K** matrix given in equation (24) can be shown to be equivalent to the Schwinger variational expression for the **K** matrix with the appropriate choice for the linear variational trial functions used in the variational expression (Nuttal 1967). This approach for computing scattering amplitudes has been found to be rapidly convergent with respect to the order of the Padé approximant in a wide variety of applications.

2.7. *Piece-wise diabatic potential*

The main focus of this paper is to examine in some detail the mechanism and qualitative characteristics of one-electron resonances. Clearly this study required a model which was simple enough to be clearly understood but included sufficient details of the full scattering problem to accurately reproduce the essential features of the resonant process. The SECP potential reproduced most of the important aspects of low-energy negative-ion shape resonances. However, we have found that the non-locality of the interaction potential made a clear identification of the mechanism for the resonant trapping difficult. Thus we further simplified the model used to study the resonances by employing the purely local potential V_{SMECP}. Although it was certainly possible that the non-locality of V_{SECP} could have provided an additional mechanism for resonant trapping, the excellent qualitative agreement between results obtained using exact exchange and local model exchange potentials gave us confidence that the resonant trapping mechanism was the same for both potentials.

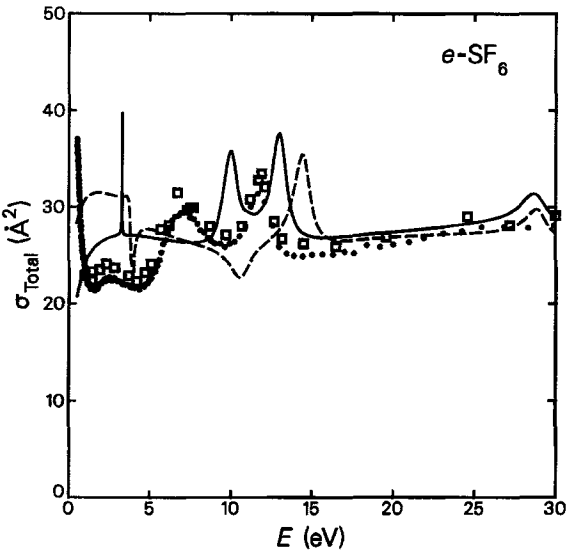

Figure 2. Total scattering-cross section for e–SF_6 collisions: (——) SECP cross-section; (– – –) SMECP cross-section; (□) experimental results (Dababneh *et al.* 1988); (●) experimental results (Kennerly *et al.* 1979).

In figure 2 we compare the SECP total electron–molecule scattering cross-sections for e–SF_6 (Gianturco *et al.* 1995) to the results obtained using the SMECP potential and to available experimental total scattering cross-sections (Kennerly *et al.* 1979, Dababheh *et al.* 1988). There were four resonances which appeared in the theoretical cross-sections. The symmetries, energies, and widths of the theoretically predicted shape resonances are given in table 2. The resonances in the SECP and SMECP cross-sections were of approximately the same width and differed in location by at most 2 eV. The agreement with experiment was similar, with the SECP resonances being a few eV higher than the three lower experimentally observed resonances. However, there is no clear experimental evidence for the resonance at 28 eV. This resonance has appeared in all other theoretical FN scattering cross-sections (Dehmer *et al.* 1978, Gyemant *et al.* 1980). The discrepancy between theory and experiment could either be due to the effects of nuclear motion or due to additional broadening of the resonant state caused by decay into other open asymptotic electronic states which were neglected in the calculation of all theoretical cross-sections reported to date. Although the agreement between the experimental and theoretical cross-sections was not quantitative, the close correspondence between experiment and theory indicated that scattering by the SMECP potential provided an accurate understanding of the mechanism of trapping of negative-ion shape resonances in electron–molecule scattering.

The standard symmetry adapted angular momentum eigenstates, $X_{lh}^{p\mu}$, which do not form the most compact angular basis set for the electron–molecule scattering problem. An alternative expansion basis set is the angular eigenfunctions obtained from diagonalizing the angular Hamiltonian at each radius r (Le Dourneuf *et al.* 1982, Lan *et al.* 1983, Battaglia and Gianturco 1989, Gianturco 1992). The angular functions obtained in this fashion are referred to as the adiabatic angular functions $Z_k^{p\mu}(\theta, \phi; r)$ which are linear combinations of the symmetry adapted harmonics

$$Z_k^{p\mu}(\theta, \phi; r) = \sum_{lh} X_{lh}^{p\mu}(\theta, \phi) C_{lh,k}(r), \tag{26}$$

where the expansion coefficients are solutions to the matrix eigenvalue equation

$$\sum_{lh} V_{l'h',lh}(r) C_{lh,k}(r) = V_k^{\mathrm{A}}(r) C_{l'h',k}(r). \tag{27}$$

The eigenvalues $V_k^{\mathrm{A}}(r)$ then form an adiabatic radial potential.

Solving the scattering equations using $V^{\mathrm{A}}(r)$ can have several advantages (Lan *et al.* 1983). First the expansion of the scattering wavefunction in adiabatic angular states converges more rapidly than the corresponding expansion in angular momentum eigenstates. Thus the number of coupled radial equations which must be solved at a certain level of accuracy is much smaller with the adiabatic basis set. The second advantage is that the numerical instabilities found in the solution of the standard momentum eigenfunction expansion given in equation (11) are greatly reduced. The third advantage is that often a single radial adiabatic potential is responsible for the appearance of a shape resonance. In such cases the adiabatic potential can be used to understand the main features of the resonant state. The spatial extent of the resonant wavefunction can be determined from the well and angular momentum barrier, and the physical mechanism for the resonant trapping is the slow rate of tunnelling through the potential barrier. One drawback to the adiabatic potential approach is that the non-adiabatic radial coupling introduces additional terms in the radial differential equations for which the standard integration method is not directly applicable.

In order to avoid the non-adiabatic coupling terms, we actually employed a piece-wise diabatic (PD) representation for the potential (Lan *et al.* 1983). In this approach the radial coordinate is divided into a number of regions so that region i is defined as $r_{i-1} < r < r_i$, where $r_0 = 0$. In each radial region we averaged the coupling potential $V_{l'h',lh}(r)$ over r and the resulting averaged potential was diagonalized as in equation (27) to yield a set of angular functions $Z^{p\mu}_{k,i}(\theta, \phi)$. Then in region i the scattering potential was transformed into the new representation in which it was nearly diagonal. The resulting equations could then be solved using the full scattering potential in each region. A further approximation we made was to ignore the off-diagonal coupling in each region. If the regions were small enough this was a very good approximation.

The key step in solving the radial equations using the PD approach was matching the radial functions and their derivatives at the boundary between radial regions. The transformation of the radial functions from one region to the next was given by the transformation matrix $U^{(i+1\leftarrow i)}_{k,k'}$ defined by

$$U^{(i+1\leftarrow i)}_{k,k'} = \sum_{lh} C^{(i+1)}_{lh,k} C^{(i)}_{lh,k'}. \tag{28}$$

When the size of the angular momentum eigenfunction basis used was larger than the size of the diabatic angular basis set, the transformation matrix $U^{(i+1\leftarrow i)}_{k,k'}$ was not in general unitary. In order for the unitarity of the **S** matrix to be maintained, it was essential to modify $U^{(i+1\leftarrow i)}_{k,k'}$ so that it was unitary. We accomplish the unitarization of $U^{(i+1\leftarrow i)}_{k,k'}$ using simple Graham–Schmidt orthonormalization on the columns of $U^{(i+1\leftarrow i)}_{k,k'}$.

To illustrate the use of the PD representation of the potential, in figure 3 we give the form of the diagonal elements of the piece-wise diabatic SME(15)CP, i.e. PDSME(15)CP, potential computed for e–SF_6 scattering for the four resonant scattering symmetries. These potentials were constructed using 27 diabatic regions between the origin and $r = 14{\cdot}2$ a.u. As can be seen in this figure, the regions were chosen so that there is no appreciable discontinuity of the diagonal elements of the potential at the region boundaries r_i. In figure 4 we compare the eigenphase sum in the t_{2g} scattering symmetry obtained from solving the full SME(15)CP potential, using the standard expansion in angular momentum eigenfunctions with 64 angular functions including all functions up to $l = 30$, with that obtained from the PD potential using 10 PD channels where the off-diagonal elements were ignored inside of each diabatic region. The scattering from the PDSME(15)CP potential is seen to have accurately reproduced the full SME(15)CP scattering results with many fewer radial channels.

2.8. *Direct determination of resonant states*

A narrow and isolated resonance in a scattering process at an energy E_R and width Γ can be shown to be due to a pole in the **S** matrix which has been analytically continued into the complex plane at an energy $E = E_R - i(\Gamma/2)$ (Taylor 1972). The **S** matrix is obtained from a scattering wavefunction by finding a solution with the asymptotic form

$$\lim_{r\to\infty} \psi_{lh,l'h'}(r) = h_l^-(kr)\delta_{ll'}\delta_{hh'} - S_{lh,l'h'} h_l^+(kr), \tag{29}$$

where $h_l^+(kr)$ and $h_l^-(kr)$ are the appropriate Hankel functions. Then it is possible to compute directly the **S** matrix at complex energy by computing the solution using the standard numerical procedures with a complex valued energy and by matching the solution to the Hankel functions with the appropriate complex argument. A resonance

energy in the scattering process can be located by finding those energies at which $0 = 1/\det \mathbf{S}$.

The approach for directly computing resonance positions by locating the poles in the **S** or equivalently the **T** matrix has been previously employed to study resonances in the photoionization process with an exact SE interaction potential. The previous application was based on the use of the Schwinger variational expression equivalent to equation (24) given above (Stratmann and Lucchese 1992). In that approach the resonance parameters are computed by locating the values of the complex energy where $\det \mathbf{D} = 0$.

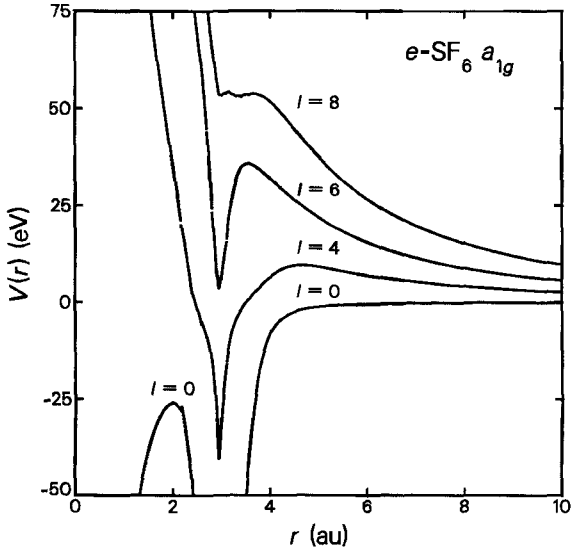

(*a*)

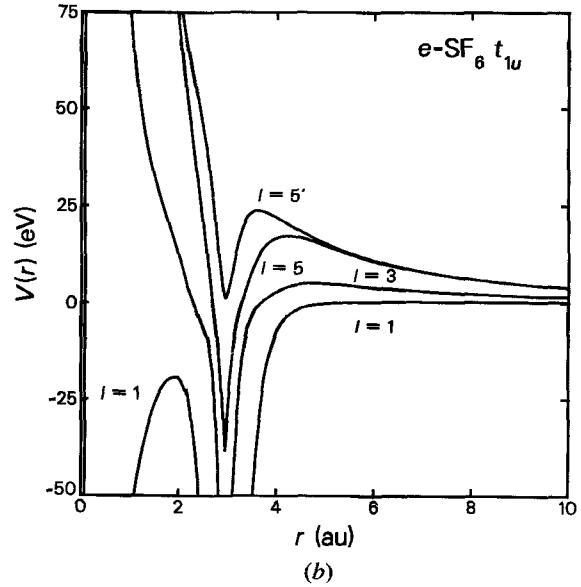

(*b*)

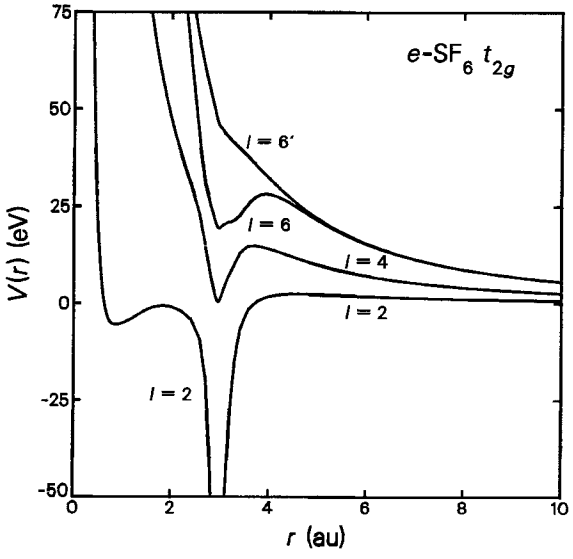

(*c*)

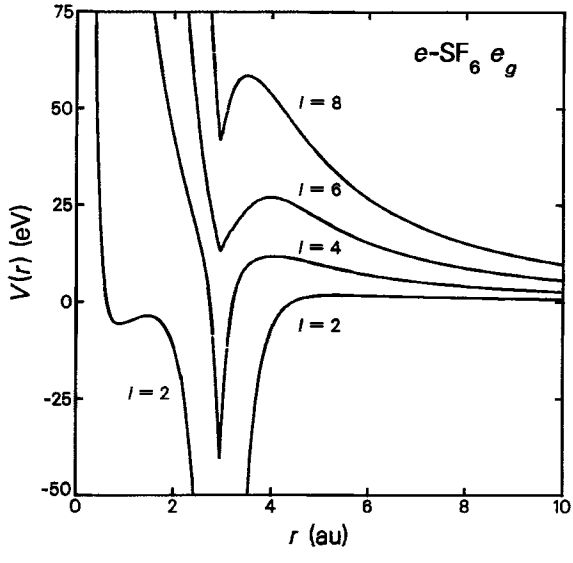

(*d*)

Figure 3. PDSME(15)CP potentials for e–SF_6 scattering. At large and small values of r the PD radial potentials given here were identical to the pure diabatic effective radial potentials one would obtain using the symmetry adapted angular momentum eigenfunctions $X_{lh}^{p\mu}$. The values of l given in the figures indicate which diabatic effective potential a particular PD potential approached at large and small values of r.

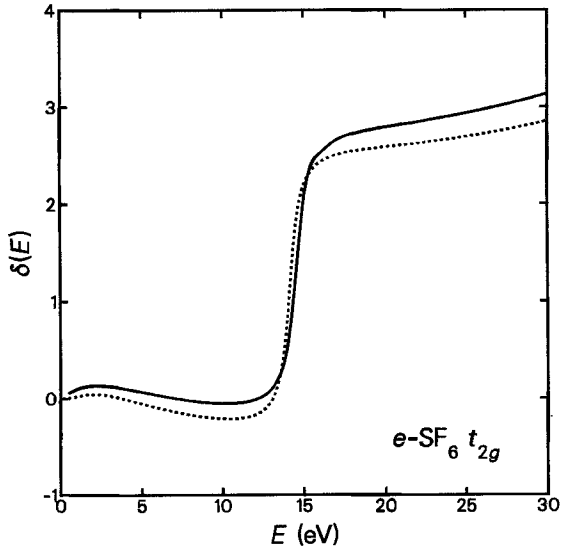

Figure 4. Comparison of eigenphase sums for e–SF_6 scattering in the t_{2g} scattering symmetry: (——) SME(15)CP potential; (- - - -) PDSME(15)CP potential.

Locating zeros in an arbitrary complex valued function of a complex argument can be a non-trivial task. The approach we used has been discussed in detail elsewhere (Stratmann and Lucchese 1992). Here we will only outline the methodology. The essential difficulty in locating the zeros of a function such as 1/det **S** is that there are generally a great many such zeros. However most of those zeros occur at energies far away from the real E axis and thus do not represent resonant scattering states. In order to define the problem, one must first identify the region in the complex plane where zeros need to be located. For example in the electron–molecule scattering problem considered here, we defined the search region as including all energies with real parts between 0·0 and 40·0 eV and with imaginary parts between 0·0 and − 25·0 eV. Within this region, a series of overlapping strips in the energy plane were defined. Within each strip we then located all zeros.

To locate the zeros within a given strip, one first computes the value of the function at a grid of energies which cover the strip. The function is then approximated in this strip by a sum of a set of orthogonal fitting polynomials whose coefficients are determined by a least-squares fit of the value of the function at the evaluation points. Typically one uses fitting polynomials which have a maximum order approximately equal to half the number of points in the fit. This implicitly allows the higher order polynomials to serve as dealiasing functions (Friesner 1986). Once the polynomial fit has been determined, all zeros of the polynomial can be located using Muller's method (Press *et al.* 1986) which is a standard root finding method. Of course one can verify that all of the roots of the polynomial have been found since the number of roots is just the order of the polynomial.

After all the zeros of the approximating polynomial have been located within the current strip of interest, the original function 1/det **S** is evaluated at the location of the estimated zeros. The new points are then added to the set of original fitting points and a new polynomial is obtained. Note that in the least-squares fitting procedure, the weight of a given point is taken to be inversely proportional to the absolute square of the

function at that point. Thus, as the location of the zeros becomes better defined, only those points near the zero will be important in the fitting process. The zeros of the new polynomial are then located. This process is repeated until the positions of the zeros have converged and the values of the actual function are sufficiently small.

Once the zeros of 1/det**S** in the region of interest have been located, the actual scattering state at that complex energy can be computed. We analysed these resonant scattering functions in terms of their radial functions and as full three-dimensional functions. One interesting observation which has been made previously is that the resonant states seem to correspond to the virtual orbitals from an MBS-SCF calculation. Here we could explicitly compare the resonant state with the virtual orbital computed in this manner. The scattering states computed in this fashion were also similar to the resonant eigenchannel functions which have been used in the study of resonant states in electron molecule scattering (Loomba *et al.* 1981). One advantage of the approach used in this study was that it avoided the ambiguity concerning which state was the resonant state. This ambiguity occurs when the resonant change in the eigenphase sum is not confined to a single eigenphase. Another advantage of the resonant state approach was that the background scattering has been removed from the scattering state thus making the resulting functions easier to interpret. Finally, as we will see below, the ability to analyse the scattering process in terms of the adiabatic scattering potentials lead to considerable insight into the mechanism for the resonant trapping.

3. Applications

3.1. *Electron–N_2 scattering*

Resonant electron scattering from N_2 is certainly the most studied electron–molecule scattering resonance (Takayanagi 1984). We have applied our procedure for studying resonances to this case to verify how well our approach reproduces the accepted understanding of the resonance in this system. The scattering resonance we have considered in this system is the $^2\Pi_g$ scattering resonance which occurs at a scattering energy of $\sim 2{\cdot}5$ eV and is due to the scattering of an electron in a π_g orbital which is trapped in an angular momentum barrier.

We have studies this resonance using the SECP and SME(2.3)CP potentials. The eigenphase sums for scattering in the π_g symmetry is given in figure 5. The computed eigenphase sums were fitted to a Breit–Wigner form to extract the resonance parameters using the functional form (Taylor 1972)

$$\delta(E) = a + b(E - E_R) + c(E - E_R)^2 + \tan^{-1}\left[\frac{\Gamma}{2(E - E_R)}\right]. \tag{30}$$

Using this functional form we found the resonance parameters for these calculations as reported in table 1. Thus we can see that the PD potential can provide a good representation of the resonant state. Additionally, we found the scattering resonance when only one PD potential was included as given in table 1. The PDSME(2·3)CP potential for the π_g scattering channel is given in figure 6. The resonance in the scattering on the single adiabatic potential was clearly due to trapping behind the barrier in the $l = 2$ adiabatic potential which had a peak value in the barrier region of 6·34 eV at $r = 2{\cdot}69$ a.u. As additional PD potentials were coupled together, the results given in table 1 show that the position and width of the resonance converged rapidly to the result obtained from the full potential. Thus we concluded in the case of the π_g resonant scattering that the mechanism for the resonant trapping was the angular momentum barrier in the adiabatic potential which asymptotically correspond to $l = 2$.

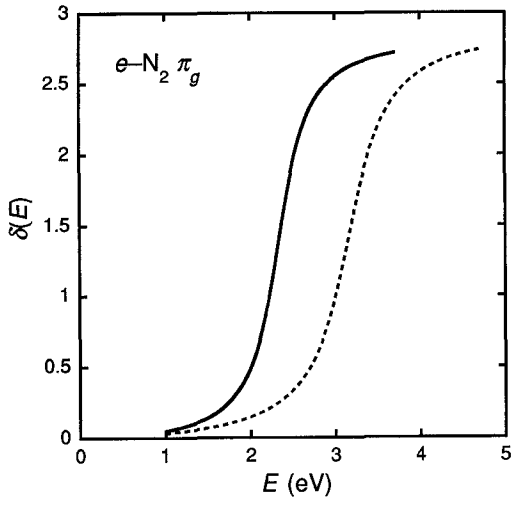

Figure 5. Comparison of eigenphase sums for e–N_2 scattering in the π_g scattering symmetry: (——) SECP potential; (- - - -) SME(2·3)CP potential.

Table 1. Position and width of resonant states in e–N_2 scattering.

Calculation	E_R (eV)	Γ (eV)
Resonances of π_g scattering symmetry		
MBS-SCF	7·70	—
PDSME(2·3)CP, $l=2$	1·56	0·14
PDSME(2·3)CP, $l=2,4$	2·94	0·58
PDSME(2·3)CP, $l=2,4,6$	3·16	0·69
PDSME(2·3)CP, $l=2,4,6,8$	3·22	0·73
PDSME(2·3)CP, all channels	3·24	0·74
SME(2·3)CP	3·16	0·70
SECP	2·33	0·53
Resonances of σ_u scattering symmetry		
MBS-SCF	30·78	—
PDSME(20)CP, $l=1,3$	15·07	3·46
PDSME(20)CP, $l=1,3,5$	21·77	6·86
PDSME(20)CP, $l=1,3,5,7$	23·85	8·58
PDSME(20)CP, all channels	24·70	9·33
SME(20)CP	24·61	9·26
SECP	23·30	12·32

It is also interesting to compare this result to that obtained using the minimum basis set calculation. In N_2 the two unoccupied valence orbitals occurred at 7·70 eV for the virtual π_g orbital and at 30·78 eV for the σ_u orbital. The π_g orbital and the resonant state obtained from the PDSME(2·3)CP potential are compared in figure 7. The phase and normalization of the resonant states were chosen by first identifying the radial distribution functions (RDF) which had the maximum peak value. Then the whole function was scaled so that the radial function with the maximum value of the RDF had a value of one at the r where the maximum in the RDF was found. Here we can see

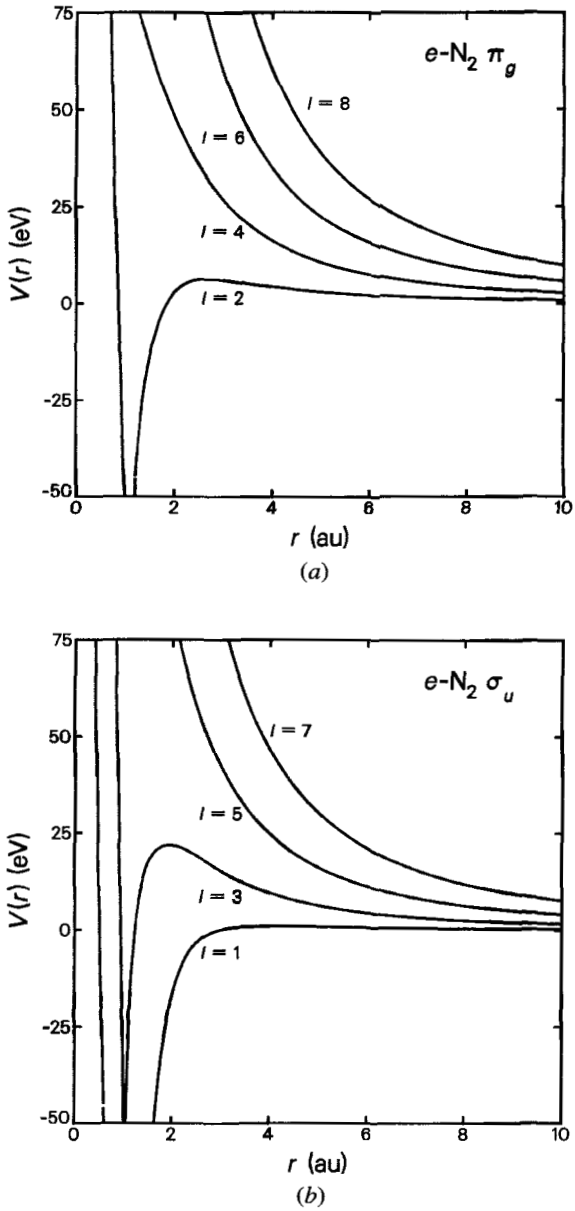

Figure 6. Piece-wise diabatic potentials for e–N_2 scattering: (*a*) PDSME(2·3)CP potential in the π_g scattering symmetry; (*b*) PDSME(20)CP potential in the σ_u scattering symmetry.

that the resonant states obtained from the MBS-SCF and the scattering calculations were nearly identical.

A resonant state corresponding to the σ_u virtual orbital was also found in the scattering calculations. As indicated in table 1, this state was very broad in the scattering calculation. It is interesting to note that none of the scattering calculations for single adiabatic potential yielded a resonance in qualitative agreement with the full scattering calculation. When the lowest two adiabatic channels were coupled together a resonant

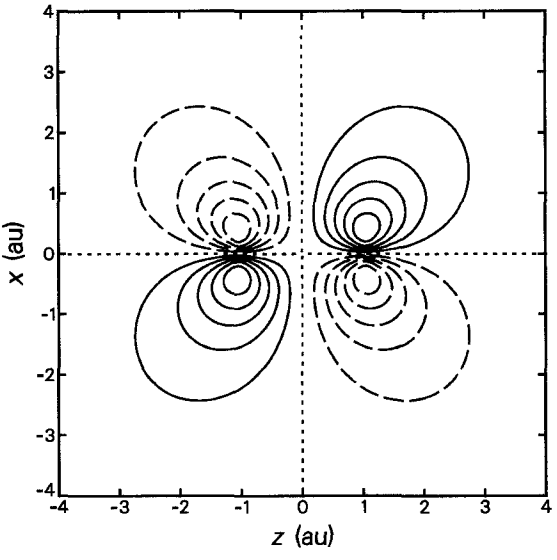

(*a*)

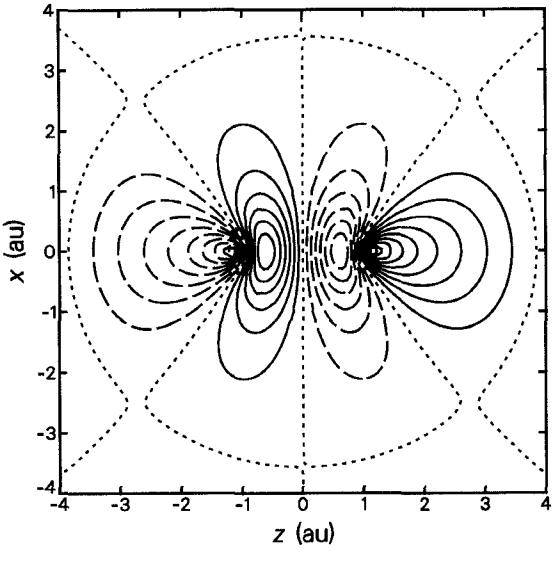

(*b*)

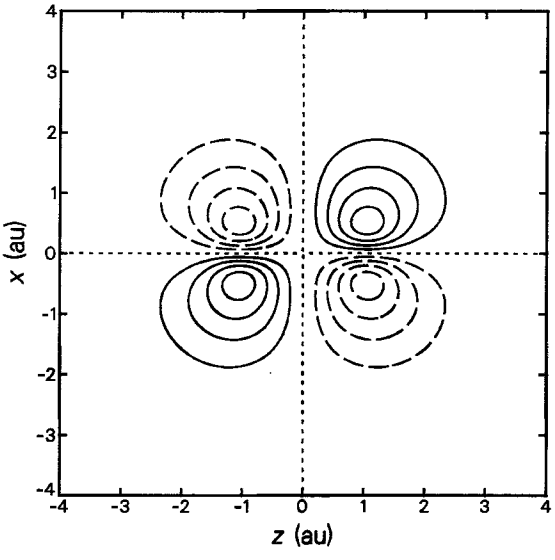

(*c*)

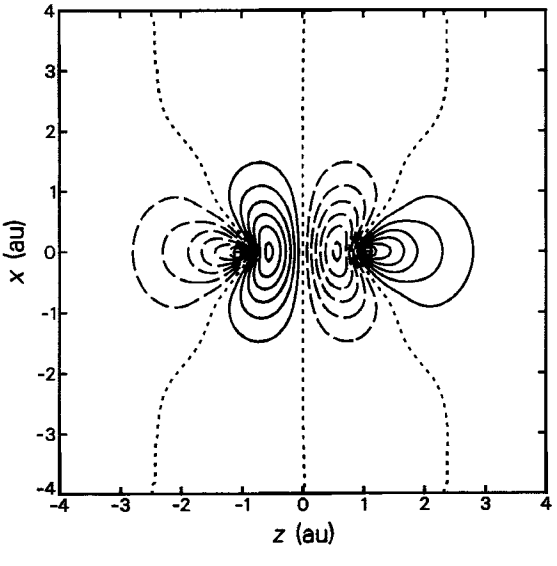

(*d*)

Figure 7. The real part of the resonant state wavefunctions in e–N_2 scattering where the dotted lines are nodes and the contours are separated by 0·1 a.u.: (*a*) PDSME(2·3)CP resonant state in π_g scattering with all channels included and with $E_R = 3{\cdot}24$ eV and $\Gamma = 0{\cdot}74$ eV; (*b*) PDSME(20)CP resonant state in σ_u scattering with all channels included and with $E_R = 24{\cdot}70$ eV and $\Gamma = 9{\cdot}26$ eV; (*c*) MBS-SCF orbital of π_g symmetry and $E = 7{\cdot}70$ eV; (*c*) MBS-SCF orbital of σ_u symmetry and $E = 30{\cdot}78$ eV.

state existed which was very similar in width and position to the resonant state in the full calculation. The resonance in the two channel calculation was below the maximum in the $l = 3$ adiabatic potential in the barrier region which was 21·83 eV at $r = 1{\cdot}96$ a.u. As further channels were coupled the result smoothly converged to the position and width found in the full SME(20)CP potential. Note that as more channels were coupled together the resonance energy actually rose above the barrier in the $l = 3$ potential. Thus the non-adiabatic coupling to the higher l channels increased the effective barrier height allowing the resonant state to be trapped at an energy where there was no apparent adiabatic potential barrier.

3.2. *Electron–SF_6 scattering*

The scattering of electrons from SF_6 has been the subject of a number of theoretical studies (Dehmer *et al.* 1978, Gyemant *et al.* 1980, Gianturco *et al.* 1995). In all studies, five prominent resonances have been found in the FN approximation. These resonances can be seen in figure 2 and have been classified by symmetry and position in table 2.

Performing an MBS-SCF (including d functions on S) calculation lead to the prediction of virtual orbitals with just the symmetries found in the scattering calculations and at the energies indicated in table 2. The MBS calculation correctly predicted the existence, symmetry, and ordering of the resonant states. However the actual energies and the spacing of these energies were much larger than that found in any of our scattering calculations. There were two sources for these differences. First the one-electron basis set is very restricted in the MBS approximation with no diffuse functions which would be needed for an accurate representation of the resonant state. Second, the MBS-SCF calculation does not include any correlation and polarization effects which were approximately included in the scattering calculations through the V_{CP} model potential. However, the MBS-SCF approach did include the essential physics needed to predict the symmetry and ordering of the negative ion resonances in e–SF_6 scattering.

It is instructive to examine the actual orbitals which were produced in the MBS-SCF calculation. In figure 8 we give contour plots of the MBS-SCF virtual orbitals. The a_{1g}, t_{1u}, and e_g orbitals are seen to be the six anti-bonding σ orbitals between the S and the F atoms. The t_{2g} orbitals are seen to be the three unoccupied d orbitals centred on the S atom. In figure 9 we present the real part of the resonant states obtained in the PDSME(15)CP calculation. Comparing the two sets of orbital plots, it is clear that basic nature of the states was the same in the MBS-SCF and PDSME(15)CP calculations. In particular, the characterization of the states in terms of the s, p, and d like behaviour around each atomic centre was the same. For example, in the t_{2g} orbital the resonant state was d like around the S atom and p like around the F atoms. The resonant PDSME(15)CP wavefunction did however give a much clearer picture about the angular behaviour of the scattered electron at large values of r. It is clear from the plots of the resonant state that the a_{1g} state was asymptotic ally $l = 4$, the e_g state was $l = 6$, and the t_{2g} state was also $l = 6$. The asymptotic behaviour of the t_{1u} state was less clear, but the location of the angular nodes indicated a combination of angular momenta including at least up to $l = 5$. This is in contrast to the dominant angular momentum we found at small r which was $l = 0$ for a_{1g}, $l = 1$ for t_{1u}, $l = 2$ for t_{2g}, and $l = 2$ for e_g. Thus from a qualitative analysis of the nodal structure of the resonant states, we see that the dominant angular momentum components changed quite dramatically from small r to large r. Thus any model which depended on a single angular momentum state, or even on a single adiabatic angular momentum state, would have missed the essential

Table 2. Symmetry, position, and width of resonances in e–SF_6 scattering.

Calculation	R_R (eV)	Γ (eV)
Resonances of α_{1g} scattering symmetry		
MBS-SCF	11·73	—
PDSME(15)CP, $l=4$	4·10	0·15
PDSME(15)CP, $l=0,4$	−0·63	—
PDSME(15)CP, $l=0,4,6$	1·39	0·28
PDSME(15)CP, $l=0,4,6,8$	2·81	0·14
PDSME(15)CP, all channels	5·37	0·33
SME(15)CP	5·40	0·38
SECP	3·30	0·032
Resonances of t_{1u} scattering symmetry		
MBS-SCF	15·89	—
PDSME(15)CP, $l=5$	12·78	1·43
PDSME(15)CP, $l=1,5$	11·71	0·63
PDSME(15)CP, $l=1,3,5$	6·41	4·34
PDSME(15)CP, $l=1,3,5,5'$	7·01	1·55
PDSME(15)CP, all channels	10·15	1·32
SME(15)CP	11·22	1·32
SECP	9·85	0·92
Resonances of t_{2g} scattering symmetry		
MBS-SCF	25·76	—
PDSME(15)CP, $l=2,4$	10·80	1·56
PDSME(15)CP, $l=2,4,6$	12·35	0·85
PDSME(15)CP, $l=2,4,6,8$	12·37	0·83
PDSME(15)CP, all channels	14·15	0·94
SME(15)CP	14·55	1·07
SECP	13·10	1·06
Resonances of e_g scattering symmetry		
MBS-SCF	39·61	—
PDSME(15)CP, $l=2,4,6$	23·74	1·43
PDSME(15)CP, $l=2,4,6,8$	24·97	1·16
PDSME(15)CP, all channels	27·15	1·07
SME(15)CP	27·60	1·17
SECP	28·84	1·89

nature of these resonances. Note that the adiabatic (or piece-wise diabatic) states suffered from this same limitation since they connect the same angular momentum states at large and small r.

In table 2 we also give the results for scattering on single PD radial potentials. For the a_{1g} and t_{1u} symmetries we found resonances which were in good agreement in energy and width to those found in the scattering calculation using the full SME(15)CP potential. In both of these symmetries the resonant state found on the single PD potential was lowered in energy when the coupling to lower energy PD potentials was included. The energy of the resonances then increased as higher energy potentials were included in the calculation. Of particular interest was the a_{1g} resonance which actually became a bound state when only the lowest two PD channels were included. Then, as coupling

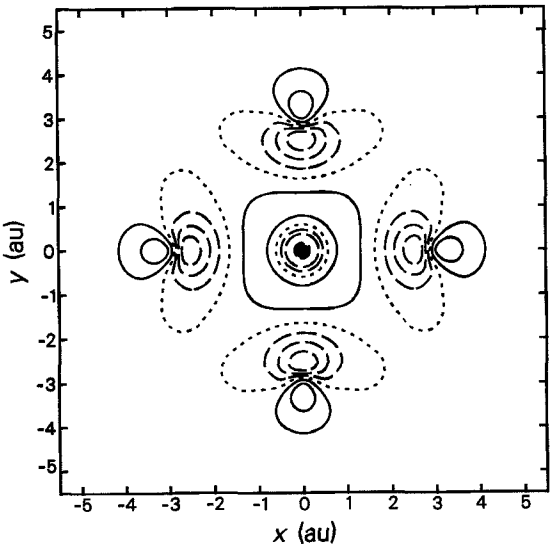

(*a*)

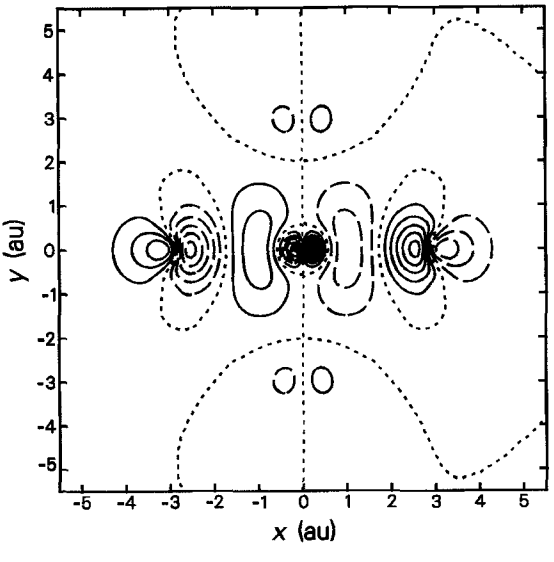

(*b*)

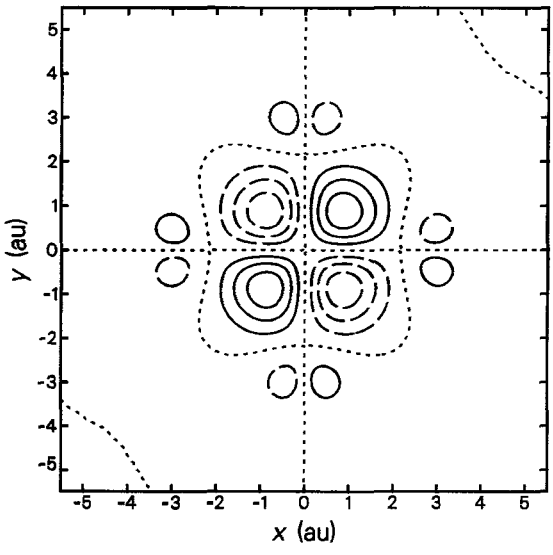

(*c*)

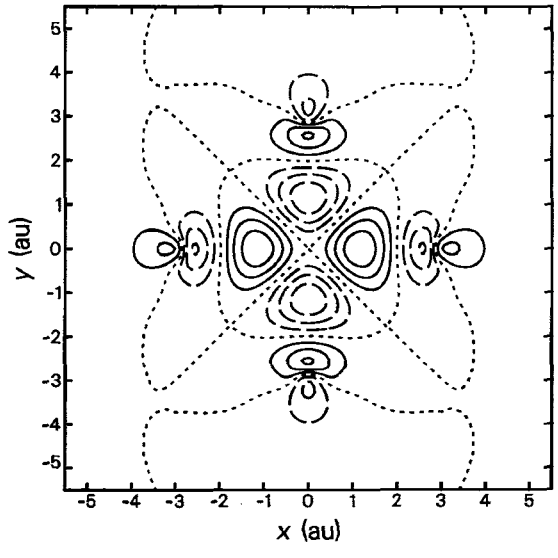

(*d*)

Figure 8. Virtual orbitals from an MBS-SCF calculation on SF_6 where the dotted lines are nodes and the contours are separated by 0·1 a.u.: (*a*) a_{1g} orbital with $E = 11{\cdot}73$ eV; (*b*) t_{1u} orbital with $E = 15{\cdot}89$ eV; (*c*) t_{2g} orbital with $E = 25{\cdot}76$ eV; (*d*) e_g orbital with $E = 39{\cdot}61$ eV.

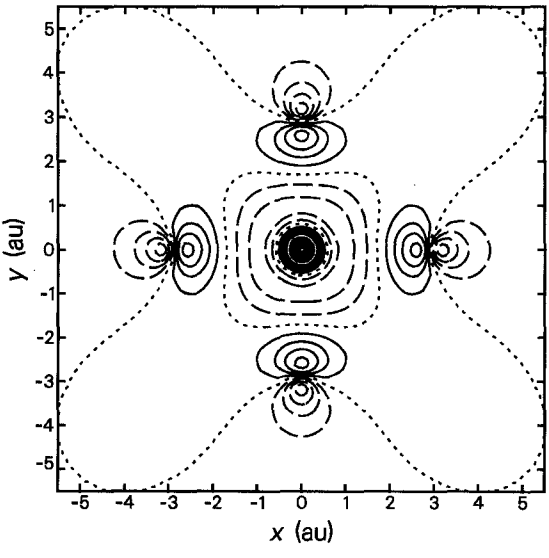

(*a*)

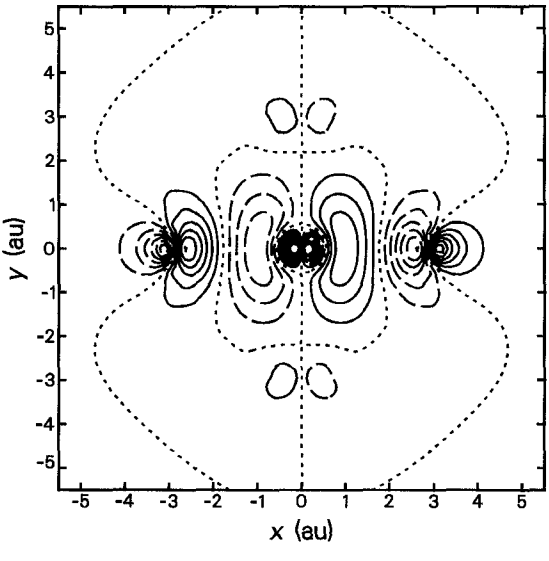

(*b*)

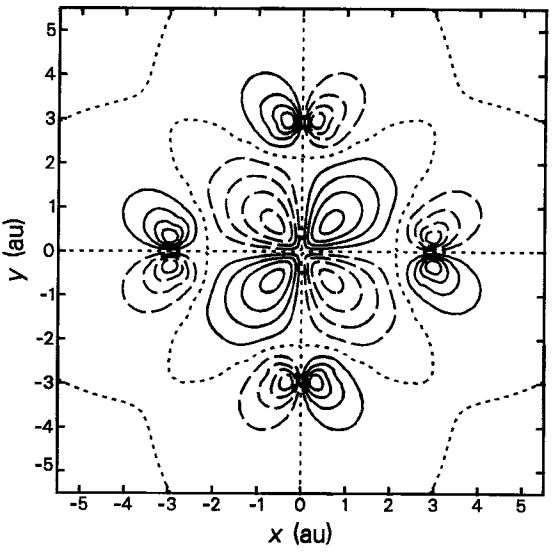

(*c*)

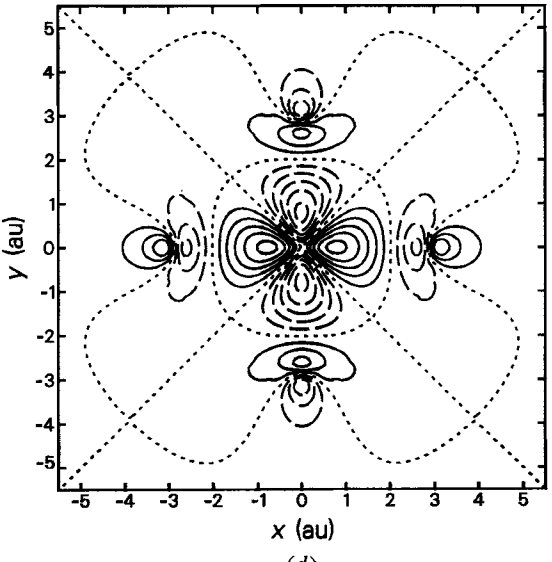

(*d*)

Figure 9. The real parts of the resonant state wavefunctions in e–SF_6 scattering using the PDSME(15)CP potential where the dotted lines are nodes and the contours are separated by 0·1 a.u.: (*a*) a_{1g} orbital with $E = 5{\cdot}37$ eV and $\Gamma = 0{\cdot}33$ eV; (*b*) t_{1u} orbital with $E = 10{\cdot}15$ eV and $\Gamma = 1{\cdot}32$ eV; (*c*) t_{2g} orbital with $E = 14{\cdot}15$ eV and $\Gamma = 0{\cdot}94$ eV; (*d*) e_g orbital with $E = 27{\cdot}15$ eV and $\Gamma = 1{\cdot}07$ eV.

to the higher PD potentials was included the state was pushed back into the continuum and again became a resonance.

As indicated in table 2, in the e_g and t_{2g} scattering symmetries we found a situation similar to that which we found with the σ_u resonance in e–N_2 scattering. In neither the e_g nor t_{2g} scattering symmetries was there a resonant state in the single adiabatic potential scattering which corresponded to the resonant state we found in the full calculation. In t_{2g} scattering symmetry, including the lowest two adiabatic radial potentials, it yielded the correct resonance, while in the e_g scattering symmetry the resonant state was not found until the lowest three adiabatic channels were coupled together. By a comparison to the behaviour of the energy of the resonant states in the a_{1g} and t_{1u} symmetries as additional channels were coupled, we see that in the t_{2g} and e_g scattering symmetries the non-adiabatic coupling created the resonant time delay in the scattering state by lowering the energy of the state below the angular momentum barrier.

Additional insight into the resonant process was gained by examining the radial distribution functions (RDFs) of the resonant states which corresponded to the contour plots given in figure 9. In figure 10 we present the lowest two RDFs for the a_{1g} resonant state. In SF_6, the F atoms are at a distance of 2·9484 a.u. from the S atom. Thus in the $l = 0$ radial function one can clearly see that the radial node at $\sim 2{\cdot}0$ a.u. was in agreement with the characterization of this state as being an anti-bonding σ virtual orbital. In these radial distribution functions there were discontinuities at each boundary between diabatic regions. The extent of the discontinuity of a given distribution function at such a boundary was then an indication of the strength of the non-adiabatic coupling in that region of the potential. As can be seen in figure 10, in the region beyond the F atoms, between 3·0 and 4·0 a.u., the non-adiabatic coupling strongly mixed the $l = 0$ and $l = 4$ adiabatic channels. The corresponding RDF in the $l = 4$ channel shows the non-adiabatic coupling for $r < 4{\cdot}0$ a.u. For $r > 4{\cdot}0$ a.u. the decaying RDF was characteristic of a wavefunction in a classically forbidden region, i.e. tunnelling. Thus we concluded that the mechanism for the resonant trapping was the non-adiabatic coupling of an $l = 0$ state in the region of the S atom with the $l = 4$ channel where the electron was trapped by the angular momentum barrier. In figure 10 (*c*) we also give the RDF for the resonant state for the $l = 4$ single adiabatic channel calculation. We can see that the $l = 4$ resonant state was very similar to the $l = 4$ component of the full resonant state. Thus an alternative mechanism for the resonant state was that the particle was trapped in the $l = 4$ resonant state with two channels for decay: tunnelling through the $l = 4$ barrier and coupling to the $l = 0$ potential on which the particle could easily escape since there was no barrier present in that potential. The value of the RDF at large r was indicative of the outward flux from the resonant state in a particular scattering channel. The fluxes on the $l = 4$ and $l = 0$ potentials were nearly equal for the a_{1g} resonance.

The RDFs for the other resonant states are given in figures 11–13. The resonance in the t_{1u} channel was very similar to that in the a_{1g} channel. The $l = 5$ potential could trap a resonance, whose RDF is shown in figure 11, which was very similar to the $l = 5$ component of the resonant state on the full potential. In the case of t_{1u} scattering, very little flux escaped by tunnelling through the barrier on the $l = 5$ potential, so that the main decay channel was through coupling to the lower l adiabatic potentials. The e_g and t_{2g} resonances were somewhat different from the other two resonances. The resonant states for both t_{2g} and e_g symmetries, shown in figures 12 and 13 respectively, had very little outgoing flux in the lowest l component. In the t_{2g} resonance, most of

the outgoing flux was in the $l = 4$ channel and in the e_g resonance most of the outgoing flux was in the $l = 6$ channel. Thus in both of these cases, the resonances was due to a non-adiabatic coupling from a low l channel in the inner region to a high l channel in the other region where the angular momentum barrier provided the trapping mechanism.

3.3. *Electron–C_6H_6 scattering*

We have also performed preliminary calculations of electron scattering from benzene. In table 3 we give the resonance energies in the MBS-SCF and PDSME(15)CP

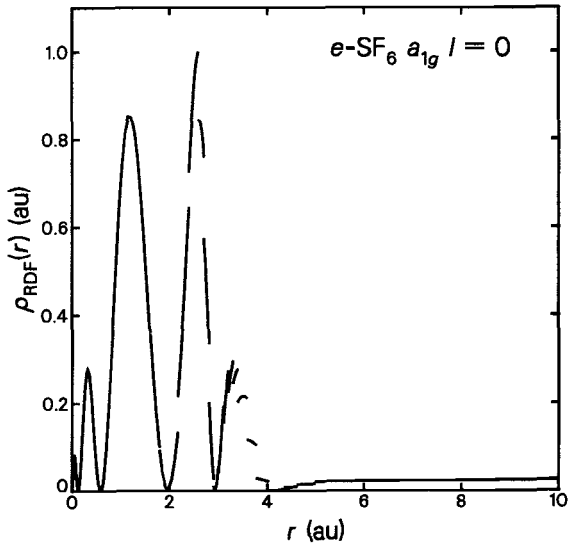

(*a*)

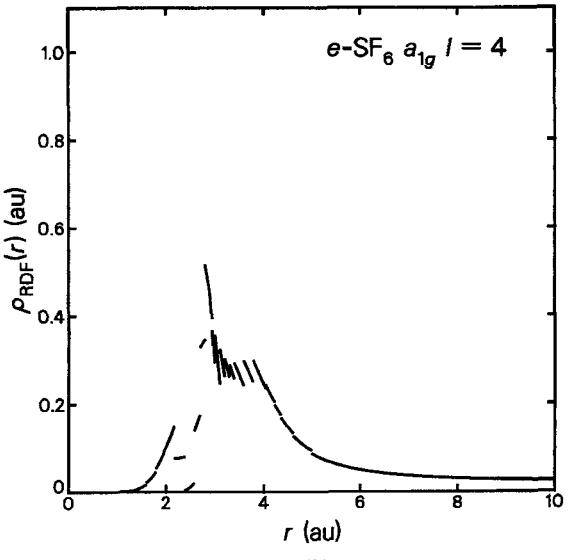

(*b*)

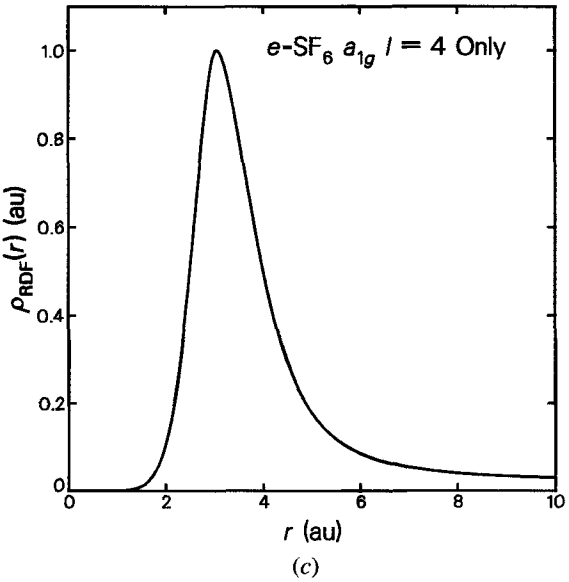

(c)

Figure 10. Radial distribution functions for a_{1g} resonant states in e–SF_6 scattering obtained with the PDSME(15)CP potential: (*a*) $l = 0$ RDF for the resonant state computed using all channels with $E = 5{\cdot}37$ eV and $\Gamma = 0{\cdot}33$ eV; (*b*) $l = 4$ RDF for the same state as in (*a*); (*c*) $l = 4$ RDF for the resonant state obtained using only one channel with $E = 4{\cdot}10$ eV and $\Gamma = 0{\cdot}15$ eV.

approximations. All correspondences indicated in the table between the MBS-SCF states and the PDSME(15)CP resonant states were assigned on the basis of energy and symmetry. With only one exception, all of the resonances using the MBS-SCF were found in the PDSME(15)CP calculation, although the ordering of the states was somewhat different in the two calculations. The lowest two resonant wavefunctions in this system were π type orbitals. All of the other resonances could be characterized as anti-bonding σ states. In figure 14 the contours of the e_{2u} and b_{2g} π resonant states obtained from the PDSME(15)CP calculation are plotted in a plane 0·75 a.u. above the plane of the molecule. These states were qualitatively in agreement with the MBS-SCF virtual orbitals. Including the plane of the molecule, which is a nodal plane for the π states, and the nodal planes evidence in figure 14, the nodal structures of the resonant states indicated that the e_{2u} resonance was trapped in an $l = 3$ angular momentum barrier and the b_{2g} state was trapped in an $l = 4$ angular momentum barrier.

Since all of the σ resonant states in e–C_6H_6 scattering were fairly broad, the resonant enhancement of the cross-sections would be overlapping. Thus in the final total cross-section few of these resonances would be expected to yield a distinct feature. One particularly interesting feature in the a_{1g} resonances was the build-up of probability density in the central region inside of the ring. In figure 15 the resonant wavefunction of the highest a_{1g} resonance is shown. The nodal structure of this state indicated that the adiabatic potential with an $l = 6$ angular momentum barrier was providing the trapping mechanism for this state. Although in e–C_6H_6 scattering this resonance was broad, it suggests the possibility of resonant states which do not correspond to valence virtual orbitals in high symmetry cage type molecules such as C_{60}.

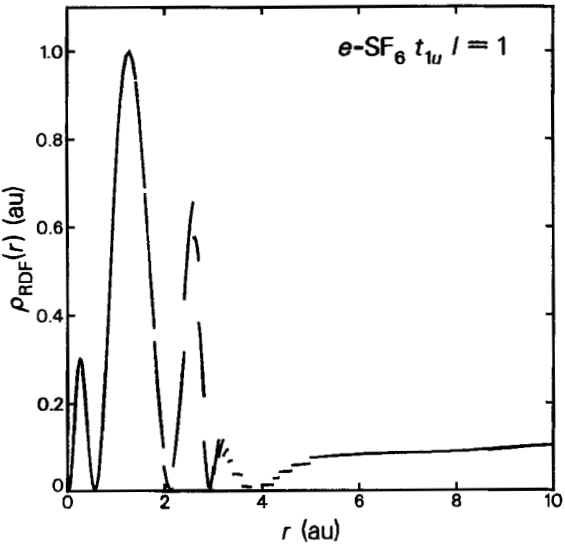

(a)

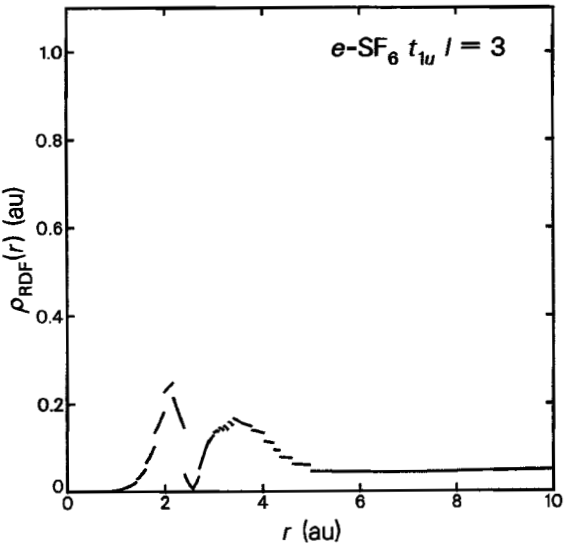

(b)

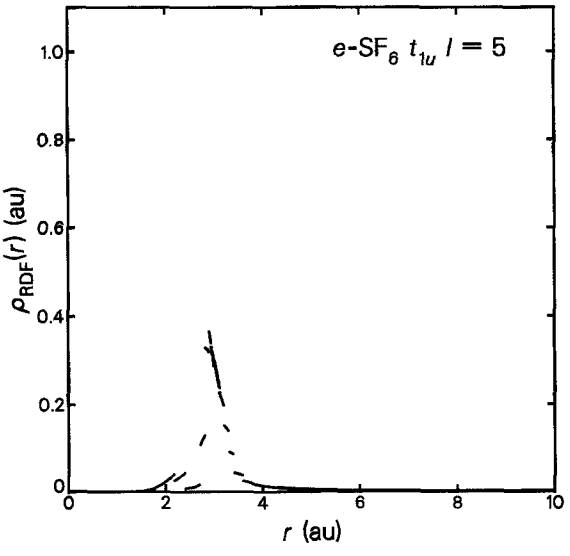

(*c*)

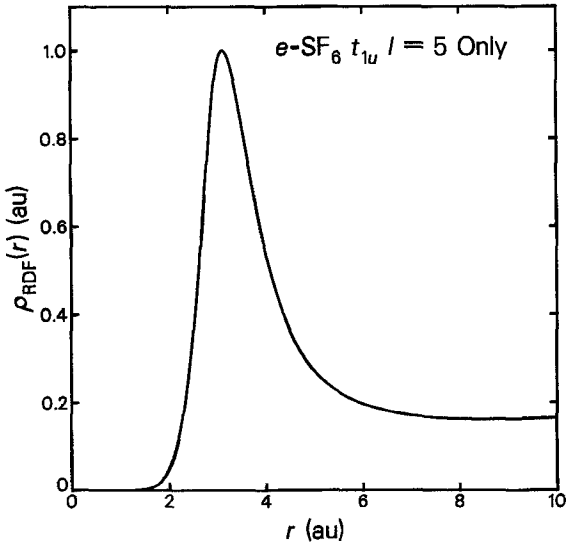

(*d*)

Figure 11. Radial distribution functions for t_{1u} resonant states in e–SF_6 scattering obtained with the PDSME(15)CP potential: (*a*) $l = 1$ RDF for the resonant state computed using all channels with $E = 10{\cdot}15$ eV and $\Gamma = 1{\cdot}32$ eV; (*b*) $l = 3$ RDF for the same state as in (*a*); (*c*) $l = 5$ RDF for the same state as in (*a*); (*d*) $l = 5$ RDF for the resonant state obtained using only one channel with $E = 12{\cdot}78$ eV and $\Gamma = 1{\cdot}43$ eV.

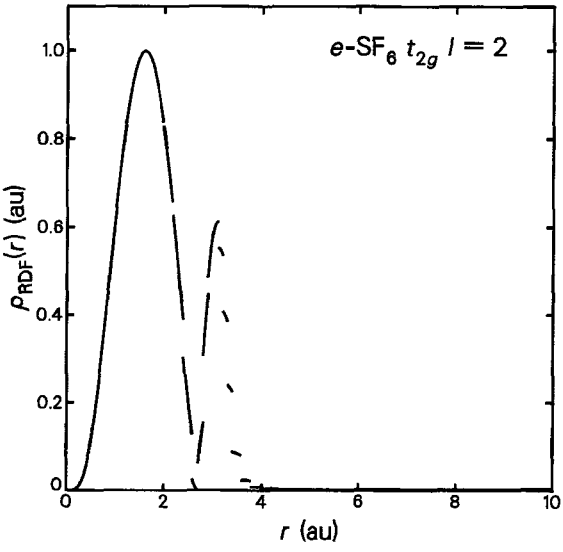

(*a*)

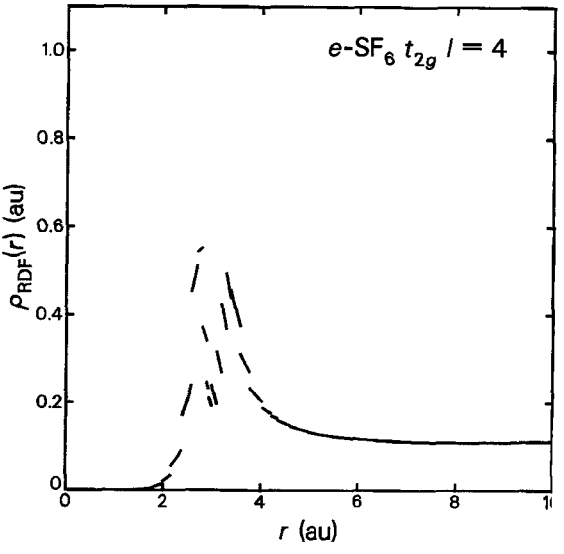

(*b*)

Figure 12. Radial distribution functions for the t_{2g} resonant state in e–SF_6 scattering obtained with the PDSME(15)CP potential: (*a*) $l = 2$ RDF for the resonant state computed using all channels with $E = 14{\cdot}15$ eV and $\Gamma = 0{\cdot}94$ eV; (*b*0 $l = 4$ RDF for the same state as in (*a*).

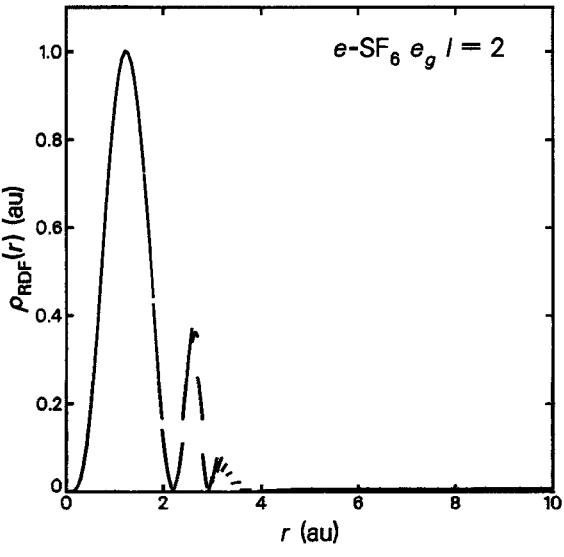

(a)

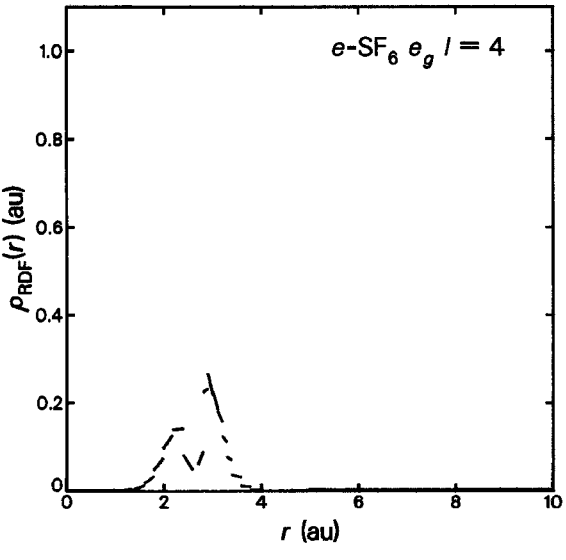

(b)

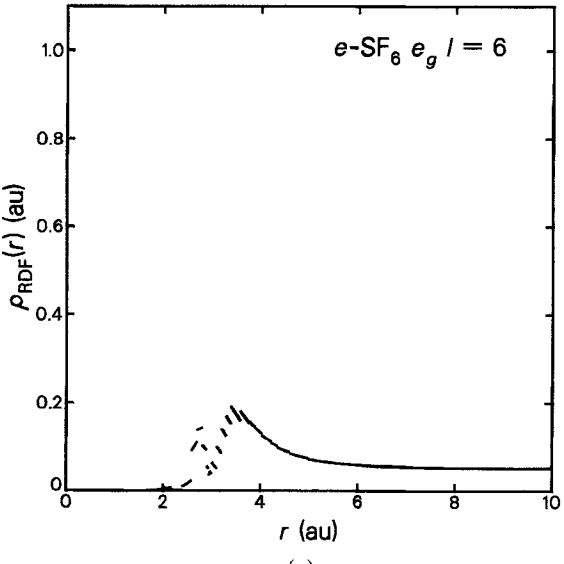

(c)

Figure 13. Radial distribution functions for the e_g resonant state in e–SF_6 scattering obtained with the PDSME(15)CP potential: (*a*) $l = 2$ RDF for the resonant state computed using all channels with $E = 27{\cdot}15$ eV and $\Gamma = 1{\cdot}07$ eV; (*b*) $l = 4$ RDF for the same state as in (*a*); (*c*) $l = 6$ RDF for the same state as in (*a*).

Table 3. Symmetry, position, and width or resonances in e–C_6H_6 scattering.

	PDSME(15)CP		MBS-SCF
Symmetry	E_R (eV)	Γ (eV)	E_p (eV)
e_{2u}	4·66	1·50	7·30
b_{2g}	9·02	2·26	13·66
e_{1u}	12·26	4·75	17·67
a_{1g}	12·32	6·78	15·79
e_{2g}	15·46	7·04	19·94
e_{2g}	—	—	24·05
b_{1u}	16·53	12·82	19·58
a_{2g}	21·49	4·82	29·48
e_{1u}	21·96	14·62	24·34
b_{1u}	24·48	5·37	31·22
a_{1g}	25·73	10·09	—

4. Conclusions

Negative ion resonances in electron–molecule scattering are the primary structural feature in the computed and measured cross-sections. Thus a detailed understanding of these resonances is essential to a complete understanding of low-energy electron–molecule scattering. The MBS-SCF calculation has been seen to predict symmetries and approximate energy of all of the important resonances in the systems considered here. In order to determine the width and trapping mechanism of the resonant state corresponding to the MBS-SCF virtual orbital, we have analysed the scattering problem using the PDSMECP model potential. The resonances due to the PDSMECP potential

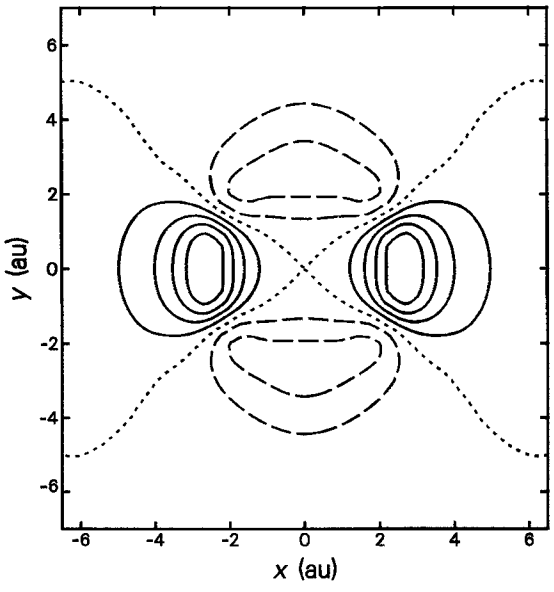

(*a*)

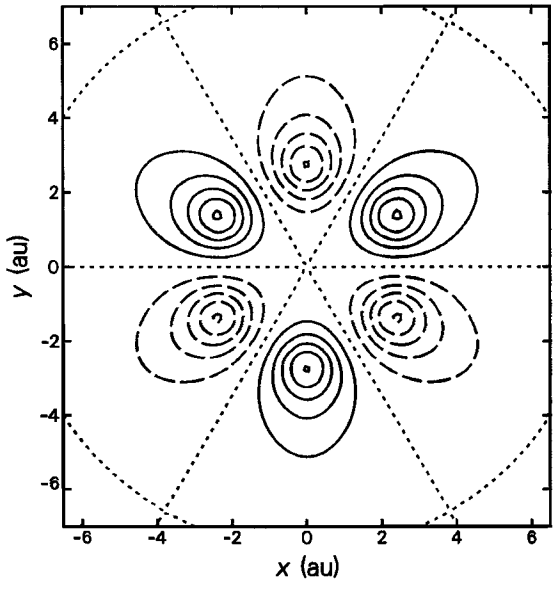

(*b*)

Figure 14. The real parts of the resonant state wavefunctions in e–C_6H_6 scattering using the PDSME(15)CP potential where the dotted lines are nodes, the contours are separated by 0·05 a.u., and $z = 0{\cdot}75$ a.u.: (*a*) e_{2u} orbital with $E = 4{\cdot}66$ eV and $\Gamma = 1{\cdot}50$ eV; (*b*) b_{2g} orbital with $E = 9{\cdot}02$ eV and $\Gamma = 2{\cdot}26$ eV.

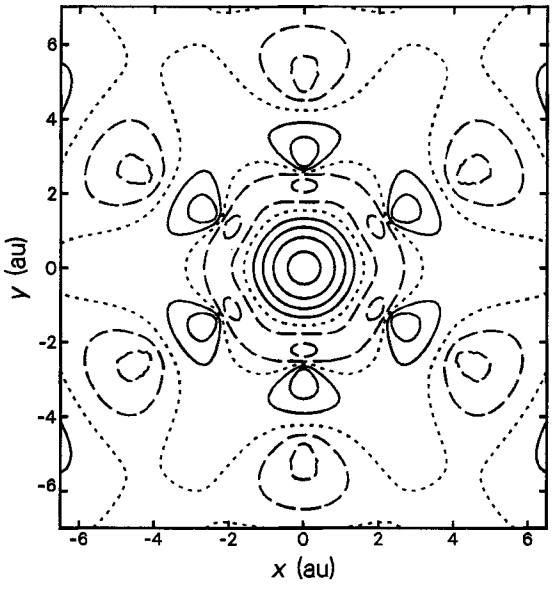

Figure 15. The real part of the resonant state wavefunction of a_{1g} symmetry in e–C_6H_6 scattering using the PDSME(15)CP potential where the dotted lines are nodes, the contours are separated by 0·1 a.u., $z = 0{\cdot}0$ a.u., and with $E = 25{\cdot}73$ eV and $\Gamma = 10{\cdot}09$ eV.

could be located using a direct search for poles of the **S** matrix in the complex energy plane. In all of the systems considered here, examination of the resonance state showed that angular momentum barriers provided the trapping mechanism. For some of the resonances, a single adiabatic potential trapped the resonant state. For other resonances, non-adiabatic coupling between a few adiabatic potentials was needed to trap the resonant state. Finally, the full SECP calculation could be performed to compare with actual experimental scattering cross-sections.

We have thus presented here a formalism which allowed the study of resonances in gas-phase molecular systems which were fairly compact and having no more than ~ 100 electrons. The combination of SECP, PDSMECP, and MBS-SCF calculations provided an interconnected set of models which could predict the location and width of the resonances and allowed a detailed understanding of the trapping mechanism. The three examples considered here illustrate the utility of this approach and indicate possible avenues for further study.

Acknowledgments

The financial support of the Italian National Research (CNR), the Italian Ministry of Scientific Research and University (MURST), and the European Community for a Research Network award are gratefully acknowledged. One of us (RRL) also wishes to acknowledge the partial support from the Robert A. Welch Foundation (Houston, Texas) under Grant No. A-1020.

References

BATTAGLIA, F., and GIANTURCO, F. A., 1989, *Europhys. Lett.*, **10,** 117.

BURKE, P. G., 1968, *Adv. atom molec. Phys.*, **4,** 173.

BURKE, P. G., and MITCHELL, J. F. B., 1974, *J. Phys.* B, **7,** 665.

CHANG, E. S., and FANO, U., 1972, *Phys. Rev.* A, **6,** 173.

DABABNEH, M, S., HSIEH, Y.-F., KAUPPILA, W. E., KWAN, C. K., SMITH, S. J., STEIN, T. S., and UDDIN, M. N, 1988, *Phys. rev.* A, **38,** 1207.

DEHMER, J. L., 1972, *J. chem. Phys.*, **56,** 4496.

DEHMER, J. L., SIEGEL, J., and DILL, D., 1978, *J. chem. Phys.*, **69,** 5205.

FRIESNER, R. A., 1986, *J. chem. Phys.*, **85,** 1462.

GARRET, W. R., 1972, *Phys. Rev.* A, **4,** 2229.

GIANTURCO, F. A., 1992, *J. molec. Struct.*, **254,** 99.

GIANTURCO, F. A., GUIDOTTI, C., and LAMANNA, U., 1972, *J. chem. Phys.*, **57,** 840.

GIANTURCO, F. A., and JAIN, A., 1986, *Phys. Rep.*, **143,** 347.

GIANTURCO, F. A., JAIN, A., and PANTANO, L. C., 1987, *J. Phys.* B, **20,** 571.

GIANTURCO, F. A., LUCCHESE, R. R., and SANNA, N., 1995, *J. chem. Phys.*, **102,** 5743.

GIANTURCO, F. A., LUCCHESE, R. R., SANNA, N., and TALAMO, A., 1994, *Electron Collisions with Molecules, Clusters, and Surfaces*, edited by H. Ehrhardt and L. A. Morgan (New York: Plenum), p. 71.

GRILL, A., 1994, *Cold Plasma in Materials Fabrication* (New York: IEEE Press).

GYEMANT, I., VARGA, Z., and BENEDICT, M. G., 1980, *Int. J. Quant. Chem.*, **17,** 255.

HALL, R. I., and READ, F. H., 1984, *Electron–Molecule Collisions*, edited by I. Shimamura and K. Takayanagi (New York: Plenum), p. 351.

HARA, S., 1967. *J. phys. Soc. Japan*, **22,** 710.

HEHRE, W. J., RADOM, L., SCHLEYER, P. V. R., and POPLE, J. A., 1986, *Ab Initio Molecular Orbital Theory* (New York: Wiley).

HERZENBERG, A., 1984, *Electron–Molecule Collisions*, edited by I. Shimamura and K. Takayanagi (New York: Plenum), p. 191.

KENNERLY, R. E., BONHAM, R. A., and MCMILAN, M., 1979, *J. chem. Phys.*, **70,** 2039.

KLONOVER, A., and KALDOR, U., 1978, *J. Phys.* B, **11,** 1623.

LAN, V. K., LE DOURNEUF, M., and LAUNAY, J. M., 1983, *Electron–Atom and Electron–Molecule Collisions*, edited by J. Hinze (New York: Plenum Press), p. 161.

LANE, N. F., 1980, *Rev. mod. Phys.*, **52,** 29.

LANGHOFF, P. W., 1984, *Resonances In Electron–Molecule Scattering, van der Waals Complexes, and Reactive Chemical Dynamics*, edited by D. G. Truhlar (Washington, D.C.: American Chemical Society), p. 113.

LE DOURNEUF, M., LAN, V. K., and LAUNAY, J. M., 1982, *J. Phys.* B, **15,** L685.

LEE, M.-T., LUCCHESE, R. R., and MCKOY, V., 1982, *Phys. rev.* A, **26,** 3240.

LESTER, W. A. JR, 1968, *J. comput. Phys.*, **3,** 322.

LOOMBA, D., WALLACE, S., and DILL, D., 1981, *J. chem. Phys.*, **75,** 4546.

LUCCHESE, R. R., and MCKOY, V., 1983, *Phys. Rev.* A, **28,** 1382.

LUCCHESE, R. R., TAKATSUKA, K., and MCKOY, V., 1986, *Phys. Rep.*, **131,** 147.

MCDANIEL, E. W., 1989, *Atomic Collisions. Electron and Photon Projectiles* (New York: Wiley).

MORRISON, M. A., and COLLINS, L. A., 1981, *Phys. Rev.* A, **23,** 127.

NATOLI, C. R., 1983, *EXAFS and Near Edge Structure*, edited by A. Bianconi, L. Incoccia and S. Stipcich (Berlin: Springer-Verlag), p. 43.

NUTTAL, J., 1967, *Phys. Rev.*, **157,** 1312.

PADIAL, N. T., and NORCROSS, D. W., 1984, *Phys. Rev.* A, **29,** 1742.

PERDEW, J. P., and ZUNGER, A., 1981, *Phys. Rev.* B, **23,** 5048.

PRESS, W. H., FLANNERY, B. P., TEUKOLSKY, S. A., and VETTERLING, W. T., 1986, *Numerical Recipes. The Art of Scientific Computing* (Cambridge University Press).

SALVINI, S., and THOMPSON, D. G., 1981, *J. Phys.* B, **14,** 3797.

SCHAEFER, H. F. III, 1972, *The Electronic Structure of Atoms and Molecules* (Reading, Massachusetts: Addison-Wesley).

SCHNEIDER, B. I., 1977, *Chem. Phys. Lett.*, **51,** 578.

SCHNEIDER, B. I., and RESCIGNO, T. N., 1988, *Phys. Rev.* A, **37,** 3749.

SHEEHY, J. A., GIL, T. J., WINSTEAD, C. L.,. FARREN, R. E., and LANGHOFF, P. W., 1989, *J. chem. Phys.*, **91,** 1796.

SHIMAMURA, I., and TAKAYANAGI, K. (editors), 1984, *Electron–Molecule Collisions* (NewYork: Plenum Press).
STRATMANN, R. E., and LUCCHESE, R. R., 1992, *J. chem. Phys.*, **97,** 6384.
SWANSON, J. R., DILL, D., and DEHMER, J. L., 1981, *J. chem. Phys.*, **75,** 619.
TAKATSUKA, K., and MCKOY, V., 1981, *Phys. Rev.* A, **24,** 2473.
TAKAYANAGI, K., 1984, *Electron–Molecule Collisions*, edited by I. Shimamura and K. Takayanagi (New York: Plenum), p. 1.
TAYLOR, J. R., 1972, *Scattering Theory* (New York: Wiley).